Modelling Radar Signal Error Performance under Atmospheric Refraction and Clutter Attenuation

Chiemela Onunka[1] and Glen Bright[2]
[1]*Discipline of Mechanical Engineering, University of KwaZulu-Natal, King George V Ave., Durban, South Africa*
[2]*Discipline of Mechanical Engineering, University of KwaZulu-Natal, Durban, South Africa*

Keywords: Error Performance, Radar Signal, Clutter Attenuation, Atmospheric Refraction.

Abstract: Radar signal error performance was modelled in the presence of atmospheric refraction and clutter attenuation. The models presented in the paper exploited prior information on atmospheric refraction properties and conditions such as partial pressure, water vapour, atmospheric temperature and the associated clutter. The atmospheric properties and characteristics were used to model random and bias errors experienced in radar systems. Errors which were associated with azimuth, elevation and target velocity were considered in the performance analysis. Range resolution and Doppler resolution were key mechanisms which were implemented in the analysis of the radar signal error performance. The radar error performance was analysed using residual error, signal-to-clutter + noise ratio and thermal noise error. Errors from azimuth, elevation and target velocity were combined in investigating the total effect of errors in determining the desired signal-to-clutter + noise ratio. The results discussed in the paper enhances target detection and tracking towards optimising the navigation system of autonomous and semi-autonomous robotic systems using radars.

1 INTRODUCTION

Radar signals are used in high-gain command-able and agile systems such as autonomous system for target detection and tracking (Chen et al., 2014). Radar systems use scanned arrays and multiple-input multiple-outputs models to increase the flexibility in the modes of operation and application (Frankford et al., 2014). Illumination of the environment with radar signals provides critical information on the energy scattered by detectable targets (Dilum Bandara et al., 2012). Scattered energy from targets and radial velocity of targets provide differentiable modes of target position and motion. Modulation of radar signals ensures accurate range determination (Hayvaci et al., 2013). Radar range and antenna characteristics provide critical information in the determination of azimuth and elevation angles of the radar system.

Resolving ambiguities associated with Doppler frequency determination ensures that targets are detected across various frequencies. The influence of detection densities allows for diversification in the detection strategies used in radar systems (Sharma et al., 2014) (Radmard et al., 2014). Timings in radar signal are influenced by the coherent and incoherent characteristics of oscillators in the radar systems. The phase reference of radar signals are hence dependent on the characteristics of the oscillators (Eustice et al., 2015) (Fellows et al., 2013).

The performance of radar system is subject to external factors such as atmospheric refraction (Panchenko et al., 2012) (Renkwitz et al., 2014) and clutter attenuation (Agarwal, et al., 2014) (Marquis, 2010). Scattering models are used to comprehend the nature and behaviour of the radar signal frequency energy distribution. Radar signals experience refraction in the elevation to and from the radar. Splaying of radar signals in the elevation plane is also another factor that occurs when radar signals are refracted. Energy absorbed by the atmosphere from the signals also affect the performance of the radar system.

The navigational systems for autonomous and semi-autonomous systems use radars for target detection and tracking. Mobile robot obstacle detection and avoidance are critical in fulfilling their navigational objectives.

The paper discusses the performance error of radar systems under atmospheric refraction and clutter attenuation. Error detection mechanisms were used in the error analysis of radar signals. The results

Onunka, C. and Bright, G.
Modelling Radar Signal Error Performance under Atmospheric Refraction and Clutter Attenuation.
DOI: 10.5220/0005957004040412
In *Proceedings of the 13th International Conference on Informatics in Control, Automation and Robotics (ICINCO 2016) - Volume 1*, pages 404-412
ISBN: 978-989-758-198-4

discussed in the paper are applicable in optimising the navigation systems of autonomous and semi-autonomous robotic systems

2 TARGET DETECTION, UNCERTAINTY AND PERFORMANCE

The technical performance of a radar system is measured in terms of distance. More specifically, the performance of radar systems are evaluated using the scatter cross-sectional area and radar range. The range scatters can be defined using different sizes. Larger range scatters are used in evaluating the performance of radar systems designed for long range detection of targets. The long range of the radar system defines the maximum range detectable by the radar system (Jang et al., 2013). The reciprocal of the time required by the radar signal to reach the maximum range and echo back is used in determining the maximum signal repetition frequency. The signal repetition frequency provides critical information in the determination of staggering for moving target. It is also used in processing moving target detector signal associated with frequency diversity. Radar range ambiguities in medium and high signal repetition frequencies can also be resolved using the repeated radar signal.

Lower range boundaries in the radar range can be created using transmit-receive switches. The mixture of long pulses and short pulses in radar systems increases uncertainty in detecting targets. Separate signals for long range mode and short range ensures that uncertainty is minimised. The amount of azimuth in the radar design influences the choice of using continuous target scanning or sector scanning in the search mode (Chen and Furumoto, 2011). Elevation properties can be introduced in the search mode or incorporated when using broad beam in the elevation plane. Broad beams in the elevation plane provide coverage to a certain height above the ground.

Detecting targets using radar signals uses definite time intervals which can be described statistically. The number of false alarms can be set at a constant value in order to ensure that false alarms are at an acceptable level and hence the probability of false alarm. Fixed number of false alarm ensures that the thresholds set for probability of false alarm is adequately optimised. Optimisation of probability of false alarm sets a threshold above the thermal noise in the radar system. A combination of radar signal and noise exceeding the set threshold yields the probability of detecting targets. The signal-to-noise ratio in the scatter provide valuable information in integrating the echoes from targets towards performance improvement of the radar system (Su et al., 2010). Distinguishing between targets and echoed signals are evaluated using the radar system angular resolution. The angular resolution is determined by reducing the azimuth and beam elevation widths. The radial velocity of the search scatter provides information on the echo Doppler frequency. The radial velocity is useful in the separation and removal of clutter in the performance analysis of the radar system.

3 ATMOSPHERIC CLUTTER MODELLING

The atmosphere refracts and absorbs energy from radar signals. The refraction sub-processes were modelled using an exponential atmospheric algorithm in determining the refractivity of radar signals in the atmosphere (Meikle, 2008). The subroutine algorithm was supplied with different input and output parameters. The exponential atmospheric model for refractivity of radar signals was expressed as:

$$N = N_s e^{-c_e h} \quad (1)$$

Where N_s represented refractivity at the earth's surface, h represented the height of the radar system above the earth's surface and c_e was a constant. Given that the refractivity of air was approximately unity, it was fitting to use the refractivity of air in the signal analysis. The refractive index of air was expressed as:

$$n = 1 + N \times 10^{-6} \quad (2)$$

The radar signal was analysed based on the point of interest (Meikle, 2008). The points of interest considered in the models were as follows:

- Radar signal analysis toward determination of target height
- Determination of classical target range
- Determination of classical target range with respect to earth's surface.
- Determination of attenuation along the radar signal

Considering radar signal as a ray, the target height h_2 was modelled as:

$$h_2 = R_2 - a \quad (3)$$

$$R_2^2 = R_1^2 + \Delta R^2 + 2R_1 \Delta R \, sin\theta_1 \quad (4)$$

Where R_2 represented the position of the radar system above the earth's surface, R_1represented the

position of the target above the earth's surface, a represented the radius of the earth and $\theta_1$represented the elevation angle. Considering the effects of partial pressure caused by water vapour e, atmospheric temperature T and signal scatter at the target position with an elevation θ; the atmospheric refractive index n was expressed as (Meikle, 2008):

$$(n-1)10^6 = N = \frac{77.6p}{T} + \frac{3.73 \times 10^5 e}{T^2} \quad (5)$$

The height of the radar system was determined using:

$$h = R\ sin\theta + \frac{R^2}{2a} \quad (6)$$

Refraction and reflection within the atmospheric layer influenced the performance of radar system. Anomalous propagation and super-refraction occurred when there was sudden variation between the layers of the atmosphere. It introduced extra clutter and blind search volume in the radar coverage area. In certain atmospheric condition, total reflection of radar signal may cause the signal to be trapped between the atmospheric layer and the earth's surface. Temperature inversions in the atmosphere can cause radar signals to be trapped or ducted. Local temperature inversion at higher altitudes are consequences of atmospheric subsidence. Temperature inversions are associated with the radar search areas experiencing high atmospheric pressures (Meikle, 2008).

Radar signals are sensitive to water vapour content in the atmosphere. Attenuation and absorption losses influenced the performance of the radar system. The model used in determining fog attenuation as a function water content M and frequency f was expressed as:

$$Fog_{Att} = 4.87 \times 10^{-4} \times M \times f^2 \ \ dB/km \quad (7)$$

Scattering and atmospheric attenuation were proportional to rain rates and drop sizes. Given that atmospheric attenuation can also be found in wet snow as result of the water content; the attenuation in wet snow was expressed as:

$$\underset{attenuation}{wet\ snow} = \frac{0.00349r^{1.6}}{\lambda^4} + \frac{0.0022r}{\lambda}\ dB/km \quad (8)$$

Where λ represented the wave length of the radar signal and r represented the water content in the snow. The radar cross section influenced the shape of scatter produced within the search area of the radar system. Scatters produced by the radar signals were usually smaller than the radar signal emitted by the transmitter. The radar cross section also determined the amplitude of the echo produced by the scatter. Weak echo signals were identified by their narrow beams and strong echoes were identified by their wide beams. The influence of these parameters were suppressed by using side-lobes with sensitive time controls. The echoes emitted by a target can be interfered with giving rise to signal fading. Scattering without fading in radar system can be optimised if targets have symmetrical shapes with determinable radar cross sections.

Polarisation of radar signals influenced the performance evaluation of the radar system. Considering the radar signals as polarised circular waves with incident radar signal rotating on reflected radar signal. The condition created a reaction radar signal which was propagated in the opposite direction. The problem was resolved by using flat and smoothly curved spherical reflectors in radar signal transmission. The spherical reflectors reversed the effects or sense of polarisation in radar signals. The echo returned from a spherical reflector having a radius ρ and normalised along its projected area $\pi\rho^2$ was expressed as (Meikle, 2008):

$$\underset{Cross-Section}{Spherical} = \frac{1}{\rho^2}\left(\left|\sum_{n=1}^{20}(-1)^n(2n+1)(a(n,\rho)+b(n,\rho))\right|\right)^2 \quad (9)$$

$$a(n,\rho) = \frac{j_n(\rho)}{j_n(\rho) - y_n(\rho)} \quad (10)$$

$$b(n,\rho) = \frac{-\frac{d}{d\rho}\rho j_n(\rho)}{\frac{d}{d\rho}\left(\rho j_n(\rho) - j\rho y_n(\rho)\right)} \quad (11)$$

Where $j_n(\rho)$ represented the spherical Bessel function of the first kind order n within the argument ρ, $y_n(\rho)$ represented the spherical Bessel function of the second kind order n within the argument ρ.

Radar systems operating at higher frequencies function adequately within an optical region. Operating the radar at lower frequencies required the incorporation of sphere sizes whose radius was four times the signal wavelength λ. Three regions provided variation parameters for radar signal performance. They were the optical region, Rayleigh and resonant region. Verifying radar signals using large spheres of radius a in the optical region was modelled as:

$$\sigma = \pi a^2\ ;\ a > 4\lambda \quad (12)$$

Analysing the radar signal under atmospheric condition such as rain within the Raleigh region was modelled as:

$$\sigma = 9\left(\frac{2\pi a}{\lambda}\right)^4 \pi a^2 \quad (13)$$

In considering scatter from targets within the radar search area interfering with each other, the signal reflections were estimated. Irregular cluster of target echoes were only constant on short radar signals. If the frequency at which the radar was operated changed, the probability distribution of the scatter was considered to be dynamic. Dynamic echo and scatter were observed using digital signal fading models in evaluating the degrees of dispersion in the probability distribution of the scatter and echo signals. Log-normal and gamma distribution were used to express the characteristics and behaviours of echoed signals and scatter. Describing clutter as a log-normal distribution, the mean-to-median ratio $e^{\frac{\sigma^2}{2}}$ of the clutter embedded in echoed signal and scatter was expressed as a log-normal distribution:

$$p(x) = \frac{1}{x\sigma\sqrt{2\pi}} exp\left(-\frac{1}{2}\left(\frac{\ln(x)-x_{median}}{\sigma}\right)^2\right) \quad (14)$$

Where σ represented the standard deviation of the signal distribution. The gamma model as function of the signal shape parameter η and signal scale parameter λ was expressed as:

$$p(x) = \frac{\lambda^\eta}{\Gamma(n)} x^{\eta-1} e^{-\lambda x} \quad (15)$$

The mean for the gamma distribution was given as:

$$mean_{Gamma} = \frac{\eta}{\lambda} \quad (10)$$

And the standard deviation for the gamma distribution was expressed as:

$$\sigma_{Gamma} = \frac{\sqrt{\eta}}{\lambda} \quad (17)$$

Clutter power spectrum was used as a measure in quantifying the effects of clutter in the performance of the radar systems. The power spectrum of clutter was the sum of fixed target and moving or random targets. Random targets were assumed to have Gaussian characteristics. The power spectrum of clutter was expressed as a function of the fixed-to-random target power ratio W^2, clutter spectrum was expressed as:

$$S_c(\omega) = \bar{\sigma}_0\left(\frac{W^2}{1+W^2}\right)\delta(\omega_0) + \frac{\bar{\sigma}_0}{(1+W^2)\sqrt{2\pi\sigma_\omega^2}} e^{\left(-\frac{(\omega-\omega_0)^2}{2\sigma_\omega^2}\right)} \quad (18)$$

Where ω_0 represented the operating frequency of the radar system, σ_ω represented the root mean square frequency spread component of the clutter model and $\bar{\sigma}_0$ represented the Weibull parameter. Given that most of the clutter can be measured with minimal operating frequency spread and zero Doppler frequency, a simper Gaussian-shaped clutter power spectrum was used and expressed as:

$$S_c(\omega) \frac{P_c}{\sqrt{2\pi\sigma_\omega^2}} e^{\left(-\frac{(\omega-\omega_0)^2}{2\sigma_\omega^2}\right)} \quad (19)$$

Where P_c represented the total clutter power.

4 RADAR ERROR CLASSES

The two major errors experienced by radar systems are random error and bias error. In normal operation, radar signal can be sent over Fraunhofer regions and the analysis of the echoes returned are done in the Fraunhofer regions. Optical calibration of radar antennas in parallel to radar beam may be in azimuth with the tilt angle. Azimuth corrections were required in order to minimise bias errors. For a surface with refractivity N_s, the atmospheric refraction model at an elevation ϕ in radian was expressed as:

$$\Delta\phi = \frac{N_s \times 10^{-6}}{tan\phi} \quad (20)$$

The atmospheric refraction was considered and included in the radar model after the radar elevation was corrected. The correction on azimuth was made directly on the radar system.

Random errors were present in the radar signal analysis as a result errors from radar signal measurements. Random errors were subject to radar signal distortion and quantisation errors. Range errors also occurred in the radar measurements. Range errors were consequences of system jitter, signal modulation timings, transmitter pulse timings, receiver delays, signal amplification variation in range estimator gates and variation in atmospheric index.

Discussing further the errors which are experienced in radar systems, the azimuth, elevation, range and target velocity each generated certain amount errors which influenced the performance of radar system. There were errors in continuous measurement of these parameters. The error signal was generated by making an angular deviation from the main axis of the radar system. The resultant error signal described the target deviation from the main axis of the radar beam. In order to perform error evaluation check, the error signal was modelled as a

linear function of the deviation angle. Azimuth ε_a and elevation ε_e errors were expressed as:

$$\varepsilon_a = \varepsilon \sin\varphi \quad (21)$$

$$\varepsilon_e = \varepsilon \cos\varphi \quad (22)$$

The azimuth and elevation errors were used in aligning the radar tracking axis on the target. Expressing amplitude modulation signal as a function of the azimuth and elevation errors:

$$E(t) = E_0\varepsilon_e \cos\omega_s t + E_0\varepsilon_a \sin\omega_s t \quad (23)$$

Where E_0 represented the error slope, ω_s represented the scan frequency and φ represented the defined angle.

5 PERFORMANCE ANALYSIS

The radar performance was evaluated in terms of the ability of the radar system to accurately identify the position of target, the resolution at which the targets were differentiated and the clutter elimination optimisation. These performance evaluations parameters were grouped into radar range, accuracy, resolution and stability. Each of these of these radar performance characteristics were influenced by atmospheric conditions and clutter attenuation.

The performance of the radar system was required to exceed the critical radar signal to background ratio in order to exceed the target detection threshold. In clear atmospheric condition, thermal noise formed the larger portion of the critical background parameter influencing performance. In addition to thermal noise was weather clutter and ground or environment clutter. Signal interference and jamming at the receiver terminal also affected the performance of radar system. Radar range in clear and stable atmospheric condition was modelled as (Mahafza and Elsherbeni, 2004):

$$Range = \left(\frac{P_t\tau_t G_t G_\gamma \sigma c^2}{(4\pi)^3 k T_n D_s L f^2}\right)^{1/4} (m) \quad (24)$$

Where τ_t represents the transmitter pulse, c represents the signal wavelength, σ represents the target cross section, k represents Boltzman's constant D_s is the chaff echo, G_t represents the transmitter gain, $G_\gamma$represents the receiver gain, P_t represents the radar power, L represents losses, T_n represents effective temperature, f represents the system's noise. The effective temperature at the receiver as influenced by atmospheric conditions was modelled as:

$$T_n = \frac{T_{output} - T_0}{L_r} + \overline{NF}\, T_0 \quad (25)$$

Where T_{output} represented the temperature at the antenna connector, T_0 represented the standard temperature in Kelvin, L_r represented the loss between the radar antenna and receiver and $\overline{NF}$ represented the receiver noise factor.

5.1 Error Detection Mechanism

Range resolution and Doppler resolution were used in the radar system error detection process. The associated accuracy and ambiguity between these two mechanisms provided valuable information in the radar system error performance evaluation. In order to determine the performance of the radar system using error analysis, integral square error was employed in the evaluation. The integral square included errors generated from range gate trigger, master signal trigger, transmitter trigger, receiver antenna, atmospheric scintillator as indicated in figure 1.

5.1.1 Range Resolution

Considering targets with zero Doppler resolution within the range ΔR. The minimum value of ΔR was used in establishing the difference between the targets. Considering the radar signal having a carrier frequency f_0, modulation amplitude $A(t)$ and phase modulation $\phi(t)$ modelled as (Mahafza and Elsherbeni, 2004):

$$s(t) = A(t)\cos(2\pi f_0 t + \phi(t)) \quad (26)$$

was expressed as the real part of a complex radar signal $\psi(t)$ where

$$\psi(t) = A(t)e^{j(\omega_0 t - \phi(t))} \quad (27)$$

It followed that

$$s(t) = Re\{\psi(t)\} \quad (28)$$

If echoes from two targets for instance with time delay τ are represented as:

$$s_{r1}(t) = \psi(t - \tau_0) \quad (29)$$

and

$$s_{r1}(t) = \psi(t - \tau_0 - \tau) \quad (30)$$

It followed that targets within the search area or range resolution were distinguished by the amount of measurable delay τ between the echoes returned by the targets. The Integral square error ε_R^2 was used to determine the variability of range between the measured target ranges. The integral square

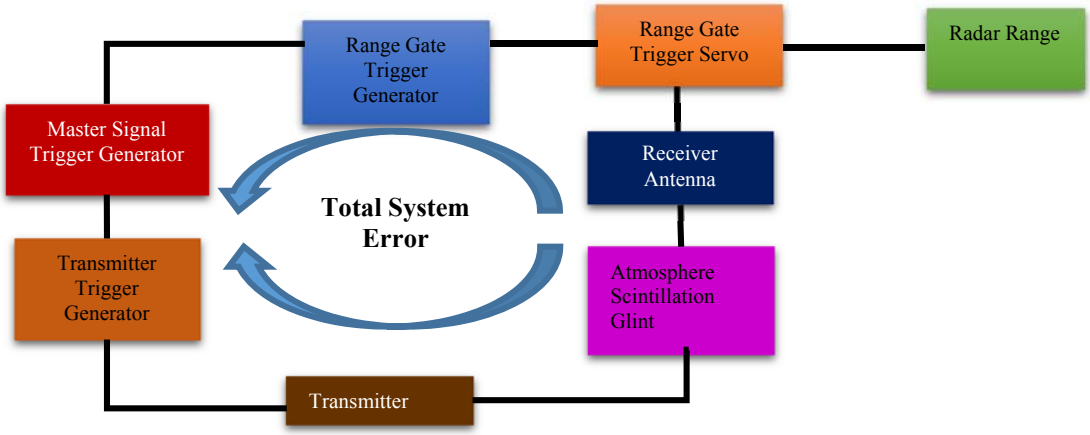

Figure 1: Integral System Components of Range Error.

between target $\psi(t)$ and $\psi(t-\tau)$ was expressed as (Mahafza and Elsherbeni, 2004):

$$\varepsilon_R^2 = \int_{-\infty}^{\infty} |\psi(t) - \psi(t-\tau)|^2 \quad dt \tag{31}$$

And was expressed further as:

$$\varepsilon_R^2 = \int_{-\infty}^{\infty} |\psi(t)|^2 \ dt + \int_{-\infty}^{\infty} |\psi(t-\tau)|^2 \ dt - \int_{-\infty}^{\infty} \{(\psi(t)\psi^*(t-\tau) + \psi^*(t)\psi(t-\tau))\ dt\} \tag{32}$$

Solving equation (27) and (32) yielded:

$$\varepsilon_R^2 = 2\int_{-\infty}^{\infty} |u(t)|^2 \ dt - 2Re\left\{\int_{-\infty}^{\infty} \psi^*(t)\psi(t-\tau)\ dt\right\} \tag{33}$$

Where

$$u(t) = A(t)e^{-j\phi(t)} \tag{34}$$

The energy carried by the radar signal was expressed by the term:

$$2\int_{-\infty}^{\infty} |u(t)|^2 \ dt \tag{35}$$

And the range ambiguity function χ_R was expressed by the term:

$$2Re\left\{\int_{-\infty}^{\infty} \psi^*(t)\psi(t-\tau)\ dt\right\} \tag{36}$$

When expressed as a function of the radar carrier frequency, the radar ambiguity function was modelled as:

$$\chi_R(\tau) = \int_{-\infty}^{\infty} u^*(t)u(t-\tau)\ dt \tag{37}$$

The radar ambiguity function had a maximum value at $\tau = 0$. Resolving targets in range was performed by computing the squared magnitude ($|\chi_R(\tau)|^2$) of the range ambiguity function. The implication of the behaviour of the range ambiguity function was that targets within the radar search area were differentiated if $|\chi_R(\tau)| \neq \chi_R(0)$ for non-zero value of the delay τ in the received target echoes. The converse behaviour of the range ambiguity function implied that targets were indistinguishable if $|\chi_R(\tau)| = \chi_R(0)$ for none zero value of delay τ. The resolution for the delay was expressed as (Mahafza and Elsherbeni, 2004):

$$\Delta\tau = \frac{\int_{-\infty}^{\infty} |\chi_R(\tau)|^2 \ d\tau}{\chi_R^2(0)} \tag{38}$$

Application of Parseval's theorem to the delay resolution yielded:

$$\Delta\tau = 2\pi \frac{\int_{-\infty}^{\infty} |U(\omega)|^4 \ d\omega}{\left[\int_{-\infty}^{\infty} |U(\omega)|^2 \ d\omega\right]^2} \tag{39}$$

The minimum resolution for the radar range

$$\Delta R = \frac{c\Delta\tau}{2} \tag{40}$$

The radar effective bandwidth was expressed as:

$$B = \frac{\left[\int_{-\infty}^{\infty} |U(\omega)|^2 \ d\omega\right]^2}{2\pi \int_{-\infty}^{\infty} |U(\omega)|^4 \ d\omega} \tag{41}$$

Hence the range as a function of signal waveform

bandwidth was expressed as (Mahafza and Elsherbeni, 2004):

$$\Delta R = \frac{c}{2B} \tag{42}$$

5.1.2 Doppler Resolution

Doppler resolution is associated with the targets radial velocity. The target radar spectrum was defined as:

$$\Psi(f) = \int_{-\infty}^{\infty} \psi(t) e^{-j2\pi ft}\ dt \tag{43}$$

Considering a target with radial velocity v as a fraction of speed of light c, frequency f_0 and wavelength λ, the Doppler shift was expressed as:

$$f_d = \frac{2vf_0}{c} \tag{44}$$

The received spectrum shifted by f_d was used to differentiate targets having different velocities and the same range values. The integral square error for the Doppler resolution was expressed as (Mahafza and Elsherbeni, 2004):

$$\varepsilon_f^2 = \int_{-\infty}^{\infty} |\Psi(f) - \Psi(f - f_d|^2\ df \tag{45}$$

Similarly, the real part of the model was modelled as:

$$2Re\left\{\int_{-\infty}^{\infty} \Psi^*(f)\Psi(f - f_d)\ df\right\} \tag{46}$$

Applying the model expressed in equation (27) yielded:

$$\Psi(f) = U(2\pi f - 2\pi f_0) \tag{47}$$

Transforming the real part the model yielded the complex correlation function:

$$\chi_f(f_d) = \int_{-\infty}^{\infty} U^*(2\pi f)U(2\pi f - 2\pi f_d)\, df \tag{48}$$

The Doppler resolution constant was expressed as:

$$\Delta f_d = \frac{\int_{-\infty}^{\infty} |\chi_f(f_d)|^2}{\chi_f^2(0)} = \frac{1}{\tau'} \tag{49}$$

The target velocity resolution as function of the target signal pulse width τ' was expressed as:

$$\Delta v = \frac{c}{2f_0\tau'} \tag{50}$$

Combining the range and Doppler resolutions, the complex envelope of the transmitted waveform was expressed as:

$$\psi(t) = u(t)e^{j2\pi f_0 t} \tag{51}$$

The delayed target signal and the Doppler shifted target signal was expressed as:

$$\psi'(t - \tau) = u(t - \tau)e^{j2\pi(f_0 - f_d)(t-\tau)} \tag{52}$$

The integral square error for the target signal was expressed as:

$$\varepsilon^2 = 2\int_{-\infty}^{\infty} |u(t)|^2\, dt - 2Re\left\{e^{j2\pi(f_0 - f_d)\tau} \int_{-\infty}^{\infty} u(t)u * (t - \tau)e^{j2\pi f_d t}\ dt\right\} \tag{53}$$

The integral squared error for the target signal was maximised by minimising the last term in equation (54). The combined Doppler and range correlation function was expressed

$$\chi(\tau, f_d) = \int_{-\infty}^{\infty} u(t)u^*(t - \tau)e^{j2\pi f_d t}\ dt \tag{54}$$

The Doppler and range resolution were maximised by minimising the modulus square of the Doppler-range correlation function.

6 SIMULATION RESULTS AND DISCUSSION

The effect of atmospheric temperature on the radar error performance results was considered in the form of thermal noise error σ_f which was described by:

$$\sigma_f = \frac{1}{1.81\tau\sqrt{2 \times SNR}} \tag{55}$$

τ represented the radar signal pulse width, SNR represented the signal-to-noise ratio of target in range. The model was used for optimum processing of thermal noise error and its effect on the radar signal error performance analysis. Targets within the atmospheric clutter were detected by using the chaff-to-signal noise ratio instead of the SNR in the thermal noise error model. The result is shown in Figure 2. The results shows that the lower chaff-to-noise ratio in dB, the higher the root mean square error of atmospheric clutter. The implication of this

result was that the performance of the radar system was optimum at higher chaff-to-noise ratio. Under this condition there were fewer probability of false alarm in target detection.

Residual error was used in determining the position array of the targets. The result is shown in figure 3. The variations on the result shown was due to noise present in the position array signal. At high gain, the error settles down quickly. The average error with small gain coefficients in the error model was approximately zero. Residual error was a measure of target tracking error as shown in figure 4.

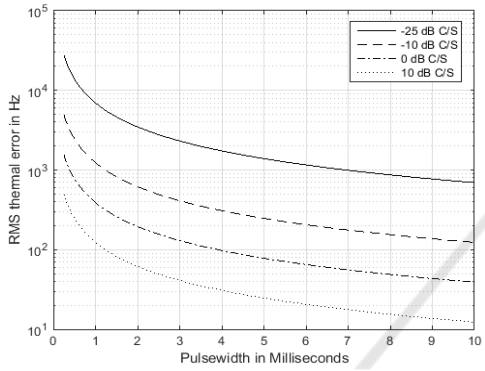

Figure 2: Error performance in clutter attenuation.

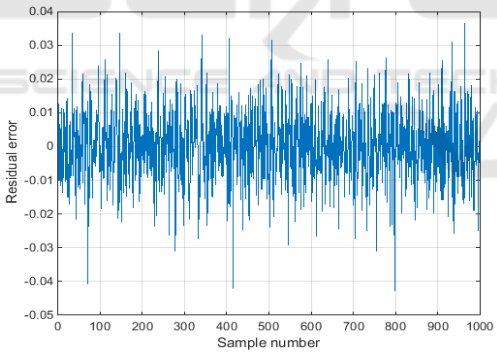

Figure 3: Residual error attenuation.

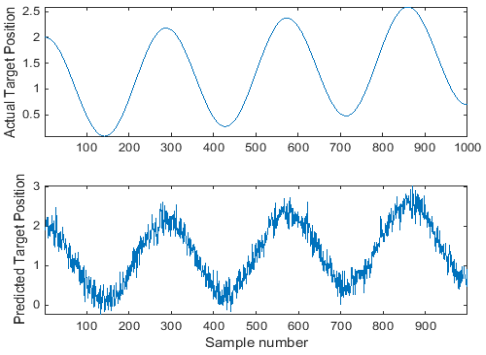

Figure 4: Target tracking attenuation.

The signal-to-noise ratio (SNR) for a target at range R was expressed as:

$$SNR = \frac{P_t G^2 \lambda^2 \sigma_t}{(4\pi)^3 R^4 k T_0 B F L} \quad (56)$$

The clutter-to-noise ratio was expressed as:

$$CNR = \frac{P_t G^2 \lambda^2 \sigma_c}{(4\pi)^3 R^4 k T_0 B F L} \quad (57)$$

And

$$SCR = \frac{SNR}{CNR} \quad (58)$$

Where P_t represented the peak power transmitted by the radar, G represented the radar antenna gain, λ represented the radar signal wavelength, σ_t represented the target radar cross section (RCS), σ_c represented the anticipated clutter RCS, k represented Boltzman's constant, T_0 represented the effective noise temperature, B represented the operating bandwidth of the radar, F represented the noise from receiver antenna and L represented the integral losses in the radar system.

In evaluating the effect of clutter in the radar signal error performance analysis, clutter characteristics were considered to be Gaussian. The radar performance accuracy was measured using a combination of returned clutter signal and noise signal referred to as Signal-to-Clutter + Noise Ratio (SIR). The SIR was computed as:

$$SIR = \frac{1}{\frac{1}{SNR} + \frac{1}{SCR}} \quad (59)$$

The results shown in figure 5 indicate that there was minimal signal degradation in the required SIR for large targets for range $R \geq 90\ km$. Figure 6 shows that there was significant signal degradation in the required SIR for small targets for range $R \geq 90\ km$. Clutter mitigation and reduction ensured that small targets were effectively detected.

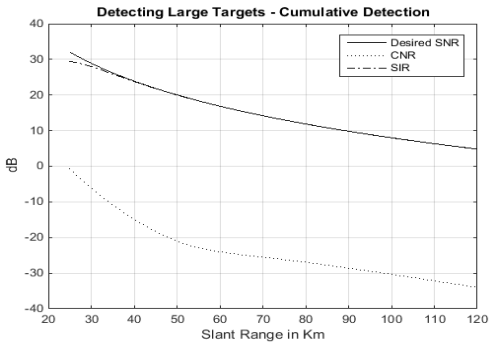

Figure 5: Clutter attenuation in large target detection.

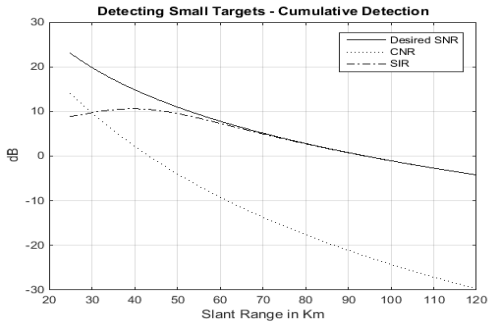

Figure 6: Clutter attenuation in small target detection.

7 CONCLUSIONS

The error performance of radar system was modelled using clutter attenuation and atmospheric refraction. The results from the simulations revealed that clutter and atmospheric refraction influenced by water vapour and temperature affected the performance of radar systems in detecting targets of various sizes. The radar signal error performance analysis was evaluated using residual error, thermal noise error and signal-to-clutter + noise ratio.

Clutter mitigation ensured that small targets can be detected at long ranges. The models presented in the paper can be applied to the control and navigation of autonomous systems using radar signals. The navigation systems of mobile robots, autonomous and semi-autonomous systems using radar for obstacle detection and avoidance can be optimised through minimisation of clutter and atmospheric refraction.

REFERENCES

Agarwal, P., Jaysaval, V. K. & Rajagopal, S., 2014. *A generalized Model for Performance Analysis of Airborne Radar in Clutter Scenario.* Noida.

Chen, J.-S. & Furumoto, J., 2011. A Novel Approach to Mitigation of Radar Beam Weighing Effect on Coherent Radar Imaging Using VHF Atmospheric Radar. *IEEE Transactions on Geoscience and Remote Sensing,* 49(8), pp. 3059-3070.

Chen, J. et al., 2014. *Surface Movement Radar Target Detection.* HangZhou, China, s.n.

Dilum Bandara, H. M. N., Jayasuman, A. P. & Zink, M., 2012. *Radar Networking in Collaborative Adaptive Sensing of Atmosphere: State of the Art and Research Challenges.* Anaheim, CA.

Eustice, D., Baylis, C., Cohen, L. & Marks, R. L., 2015. *Effects of Power Amplifier Nonlinearities on the Radar Ambiguity Function.* Arlington, VA.

Fellows, M., C, B., Cohen, L. & J, M. R., 2013. *Calculation of the Radar Ambiguity Function from Time-Domain Measurement Data for Real-Time, Amplifier-in-the-Loop Waveform Optimization.* Columbus, OH.

Frankford, M. T., Stewart, K. B., Majurec, N. & Johnson, J. T., 2014. Numerical and Experimental Studies of Target Detection with MIMO Radar. *IEEE Transactions on Aerospace and Electronic Systems,* 50(2), pp. 1569-1577.

Hayvaci, H. T., De Maio, A. & Erricolo, 2013. Improved Detection Probability of a Radar Target in the Presence of Multipath with Prior Knowledge of the Environment. *IET Radar, Sonar & Navigation,* 7(1), pp. 36-46.

Jang, Y., Lim, H., Oh, B. & Yoon, D., 2013. *Clutter Mapping and Performance Analysis for Vehicular Radar Systems.* Belgrade.

Mahafza, B. R. & Elsherbeni, A. Z., 2004. *Simulations for Radar Systems Design.* Boca Raton: Chapman & Hall/ CRC Press LLC.

Marquis, E., 2010. *Antenna Size Versus Sea Clutter Rejection: A new Analysis of Coastal Radar performances and Optimization.* Paris.

Meikle, H., 2008. *Modern Radar Systems.* 2nd ed. Boston: Artech House Inc..

Panchenko, A. Y., Slipchenko, N. I. & Liu, C., 2012. *Comparison of Radar and Acoustic Methods for Atmopshere Sounding.* Sevastopol, Crimea, s.n.

Radmard, M., Chitgarha, M. M., Nazari Majd, M. & Nayebi, M. M., 2014. *Ambiguity Function of MIMO radar with Widely Separated Antennas.* Gdansk.

Renkwitz, T., Stober, G., Chau, J. L. & Latteck, R., 2014. *Estimation and Validation of the Radiation Pattern of the Middle Atmosphere Alomar Radar System (MAARSY).* Beijing.

Sharma, G. V. K., Srihari, P. & Rajeswari, K. R., 2014. *MIMO Radar Ambiguity Analysis of Frequency Hopping Pulse Waveforms.* Cincinnati, OH, .

Su, X., Wu, Z. & Zhang, Y., 2010. *Detection Performance of C-Band Radar in Sea Clutter.* Guangzhou.